JACS
JOURNAL OF THE AMERICAN CHEMICAL SOCIETY

COMMUNICATION

pubs.acs.org/JACS

Nanocrystals Composed of Alternating Shells of Pd and Pt Can Be Obtained by Sequentially Adding Different Precursors

Hui Zhang,[†,‡] Mingshang Jin,[†] Jinguo Wang,[§] Moon J. Kim,[§] Deren Yang,[‡] and Younan Xia*[,†]

[†]Department of Biomedical Engineering, Washington University, St. Louis, Missouri 63130, United States

[‡]State Key Laboratory of Silicon Materials and Department of Materials Science and Engineering, Zhejiang University, Hangzhou, Zhejiang 310027, People's Republic of China

[§]Department of Materials Science, University of Texas at Dallas, Richardson, Texas 75083, United States

Supporting Information

ABSTRACT: This paper describes a layer-by-layer epitaxial approach to the synthesis of multishelled nanocrystals composed of alternating shells of Pd and Pt by starting with seeds made of Pd or Pt nanocrystals. The synthesis was conducted by sequentially adding $PtCl_4^{2-}$ and $PdCl_4^{2-}$ salt precursors into a system containing either Pd or Pt seeds (in the shape of cuboctahedrons, octahedrons, plates, or cubes) together with a weak reducing agent such as citric acid (CA). The slow reduction kinetics associated with CA played an important role in the epitaxial growth of one metal on the other, resulting in the formation of Pd−Pt multishelled nanocrystals. Owing to the capping effect of CA for {111} facets of Pd and Pt, the multishelled nanocrystals tended to be enclosed by {111} facets in the form of octahedrons or thin plates, depending on the shapes of the Pd or Pt seeds: octahedrons for cuboctahedral, cubic, or octahedral seeds, and plates for platelike seeds.

Over the past decade, core−shell nanocrystals consisting of two different metals have received great interest because of their unique properties originating from the electronic coupling between the metals and a wide variety of promising applications in plasmonics, catalysis, and hydrogen storage.[1−7] To this end, bimetallic core−shell nanocrystals with well-defined shapes have been synthesized from noble metals such as Au, Ag, Pd, and Pt through heteroepitaxial growth of one metal on the surface of seeds made of another metal.[8−11] For example, Yang and co-workers have demonstrated the synthesis of Pt−Pd core−shell nanocrystals in the shape of cube, cuboctahedron, and octahedron using seed-mediated epitaxial growth.[12] Han and co-workers reported the synthesis of Au−Pd core−shell octahedrons through a coreduction method with cetyltrimethylammonium chloride (CTAC) as both the reducing agent and stabilizer.[13] Xie and co-workers described the formation of rectangular Au−Pd core−shell nanorods enclosed by {100} facets through the growth of a Pd shell on the {110} and {100} facets of Au nanorods.[14] As proposed by Tian and co-workers,[15] heteroepitaxial synthesis of bimetallic core−shell nanocrystals in a solution phase is limited by a set of specific conditions: (i) there must be a small (typically <5%) mismatch in lattice constants between the core and shell metals; (ii) the metal for shell must have a lower electronegativity than the metal for core; (iii) there should be a smaller bonding energy between shell atoms than between core and shell atoms. In these regards, it seems to be impossible to grow multishelled nanocrystals comprising alternating layers of two different noble metals (marked by A and B) because the bonding energy of A to B is always larger than that of either A to A or B to B, together with a higher electronegativity for either A than B or B than A.

For a system involving Pd and Pt, Pd−Pt bimetallic nanodendrites were usually obtained when seeds made of Pd nanocrystals were used with a relatively strong reducing agent such as ascorbic acid (AA) due to the following order in bonding energies: E_{Pt-Pt} (307 kJ/mol) > E_{Pt-Pd} (191 kJ/mol) > E_{Pd-Pd} (136 kJ/mol).[16] In parallel, we have also successfully achieved epitaxial overgrowth of Pt shells on well-defined Pd nanocrystals by using citric acid (CA) as both reducing and capping agents.[17,18] This reduction offers a potential route to the synthesis of Pd−Pt multishelled nanocrystals. We believe that the slow reduction kinetics of a Pt or Pd precursor by CA is instrumental to the epitaxial growth of a Pt shell on a Pd seed, and vice versa.[19] In this communication, we report the first demonstration of heteroepitaxial growth of Pd−Pt (or Pt−Pd, depending on the starting seed) multishelled nanocrystals by sequentially adding Pt and Pd salt precursors into an aqueous solution containing Pd or Pt seeds with CA as both capping and reducing agents. We chose Pd and Pt as our focus because nanocrystals made of these two metals have been of great interest, owing to their widespread applications in catalysis and electrocatalysis.[20−22] In addition, the multishelled nanocrystals composed of alternating Pd and Pt layers are of particular interest for possible new features arising from the effective coupling between adjacent layers.

Figure 1 schematically shows how multishelled nanocrystals are obtained by alternating the deposition of Pt and Pd shells on a seed of Pd cuboctahedron. The key to the success of this synthesis is the use of CA as both reducing and capping agents. As a relatively weak reducing agent, CA can generate Pt and Pd atoms at the right pace to ensure layered, epitaxial growth between these two metals. In addition, the lack of a galvanic replacement between Pd and a Pt salt precursor in the absence of Br^- ions, as discussed in our previous report,[23] and the negligible lattice mismatch between Pd and Pt (only 0.77%) are of critical importance to the formation of Pd−Pt multishelled nanocrystals in high quality. As shown in Figure 1, the epitaxial growth of a Pt

Received: May 15, 2011
Published: June 16, 2011

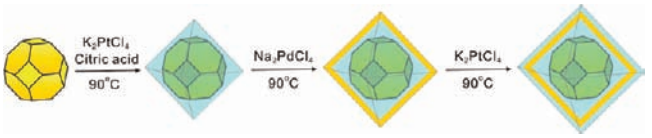

Figure 1. Layer-by-layer epitaxial growth of Pd−Pt multishelled nanocrystals with a Pd cuboctahedron serving as the seed. The success of this synthesis relies on the use of citric acid as both the reductant and capping agents to ensure a conformal growth.

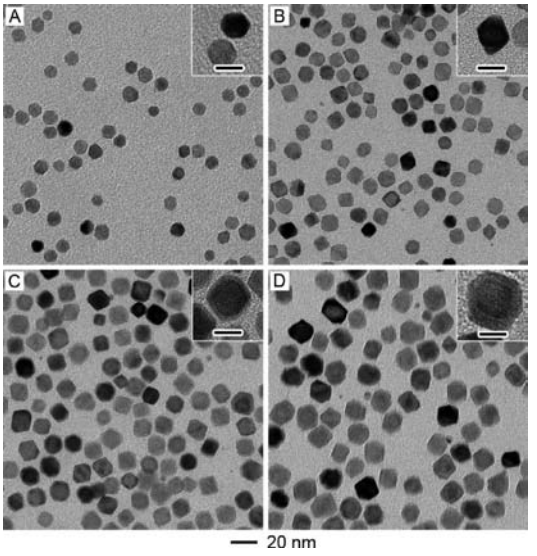

Figure 2. (A) TEM image of Pd cuboctahedrons of 9 nm in size that served as the seeds in the growth steps. (B−D) TEM images of (B) Pd@Pt, (C) Pd@Pt@Pd, and (D) Pd@Pt@Pd@Pt nanocrystals prepared using the standard procedure. (Insets) TEM images of individual nanocrystals at a higher magnification. Scale bars are 10 nm.

shell on a Pd cuboctahedron is achieved by reducing K_2PtCl_4 with CA, leading to the formation of a Pd@Pt core−shell nanocrystal with an octahedral shape. The selective adsorption of CA on {111} facets of Pt is responsible for the morphological transition from a cuboctahedron to an octahedron due to a faster growth along the ⟨100⟩ direction. In the following steps, Pd and Pt are sequentially deposited on the {111} facets to generate an octahedral nanocrystal with an alternating distribution for the Pt and Pd shells. Experimental details for the syntheses of Pd or Pt seeds and Pd−Pt multishelled nanocrystals can be found in the Supporting Information (SI).

Figure 2 shows TEM images of the products obtained at different stages of heteroepitaxial growth involving sequential addition of Pt and Pd salt precursors at 90 °C in the presence of CA. The Pd cuboctahedrons with an average size of 9 nm (Figure 2A) were prepared, using a procedure previously reported by our group,[19] and then were employed as seeds to induce/direct the epitaxial growth of Pt. After the reaction had proceeded for 9 h in an aqueous solution containing 300 mg of CA, 14 mg of K_2PtCl_4, and 1 mL of the suspension of Pd cuboctahedrons, Pd@Pt octahedrons with an average size of 12 nm were obtained (Figure 2B). A morphological transition from cuboctahedrons to octahedrons suggests a faster growth rate along ⟨100⟩ direction than ⟨111⟩ direction for the Pt due to

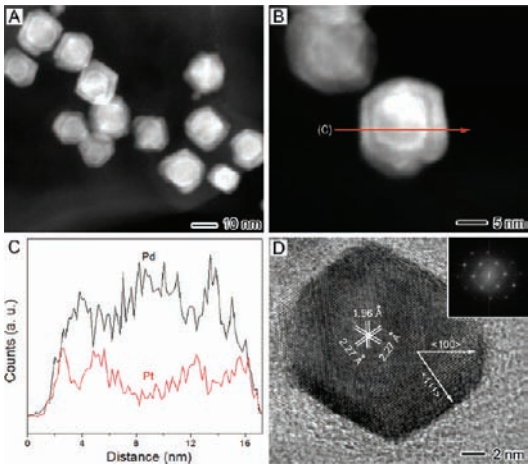

Figure 3. Morphological, structural, and compositional characterizations of the triple-shelled nanocrystals in Figure 2D, which were prepared using the standard procedure: (A, B) STEM images, (C) line-scan EDX spectrum of an individual nanocrystal as indicated in (B), and (D) high-resolution TEM image. Fourier transform (FT) pattern of an individual triple-shelled nanocrystal shown in (D) recorded along the ⟨110⟩ zone axis.

the preferential adsorption of CA on the {111} facets.[24] The difference in size between cuboctahedrons and octahedrons suggests the epitaxial growth of Pt shells with a thickness of 1−2 nm on the {111} facets of Pd seeds, which is similar to what we reported for the growth of Pt shells on Pd plates.[18] In the next step, 24 mg of Na_2PdCl_4 was added into the reaction system for epitaxial growth of Pd shells on the Pd@Pt core−shell octahedrons (Figure 2C). From this image, it is clear that the octahedral shape of the Pd@Pt core−shell nanocrystals formed in the first step was essentially retained during the formation of Pd shells while the size was increased to 16 nm. As shown by a magnified TEM image in the inset of Figure 2C, the nanocrystal comprised three regions with different contrasts in the sequence (starting from the center) of bright, dark, and bright, corresponding to the Pd seed, Pt shell, and Pd shell, respectively. The Pd shell was about 2 nm in thickness, as obtained by comparing the size of Pd@Pt@Pd octahedrons with that of Pd@Pt octahedrons. In the third step, another new shell of Pt was deposited, as shown in Figure 2D, on the surface of the Pd@Pt@Pd concentric nanocrystals by adding 21 mg of K_2PtCl_4 into the same reaction system. In this case, the octahedrons were slightly truncated at corners with an average size of 20 nm. The magnified TEM image (inset of Figure 2D) shows an alternating distribution of four regions with different contrasts, implying the formation of Pd@Pt@Pd@Pt triple-shelled nanocrystals. We believe that the method presented here can be further extended to generate core−shell nanocrystals with more Pd and Pt shells by repeating the aforementioned deposition procedures. In addition to the use of Pd cuboctahedrons as seeds for the alternating deposition of Pt and Pd shells, Pd octahedrons (Figure S1, SI) and plates (Figure S2, SI) have also been employed to synthesize Pd−Pt multishelled nanocrystals with other different shapes.

We further used high-angle annular dark-field scanning transmission electron microscopy (HAADF-STEM), energy dispersive X-ray (EDX), X-ray diffraction (XRD), and high-resolution transmission electron microscopy (HRTEM) to characterize the morphology, structure, and composition of the

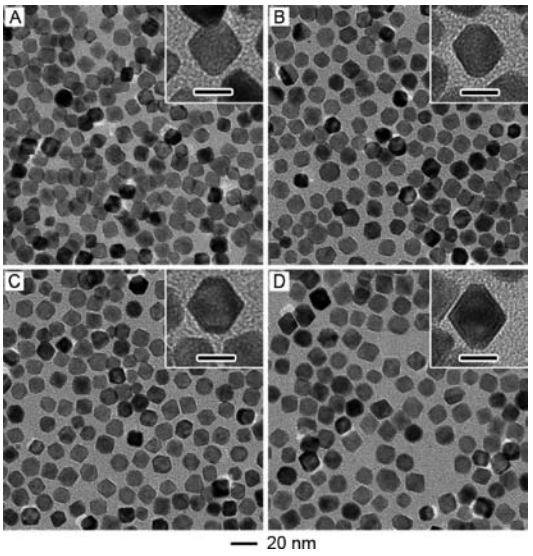

Figure 4. TEM images of Pd@Pt@Pd double-shelled nanocrystals with the Pd layers being different thicknesses by adding different amounts of Na_2PdCl_4: (A) 2.4, (B) 4.8, (C) 9.6, and (D) 38.4 mg. (Insets) TEM images of individual nanocrystals at a higher magnification. Scale bars are 10 nm.

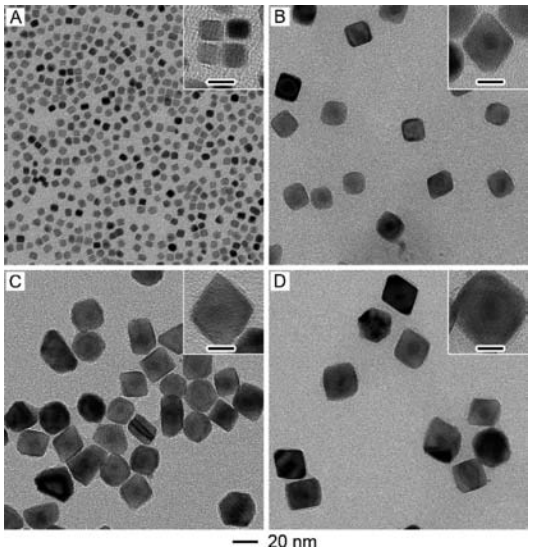

Figure 5. (A) TEM image of Pt cubes 5 nm in edge length that served as the seeds for the growth steps. (B–D) TEM images of (B) Pt@Pd, (C) Pt@Pd@Pt, (D) Pt@Pd@Pt@Pd nanocrystals prepared using the standard procedure, except for the use of the Pt cubes as the seeds and the addition of Pd and Pt precursors in a sequence of 24 mg Na_2PdCl_4, 14 mg K_2PtCl_4, and 24 mg Na_2PdCl_4. (Insets) TEM images of individual nanocrystals at a higher magnification. Scale bars are 10 nm.

Pd@Pt@Pd@Pt core–shell nanocrystals. The HAADF-STEM image in Figure 3A clearly shows the triple-shelled structure of Pd@Pt@Pd@Pt octahedrons with some truncation at corners. The compositional distribution of each element in the triple-shelled octahedron was revealed by EDX line-scan analysis. Figure 3C shows a line-scan EDX spectrum of elemental Pd and Pt that was recorded through the center of an individual nanocrystal (marked by an arrow in Figure 3B). As can be seen, the Pd trace has three peaks, while the Pt trace has four peaks (Figure 3C). Careful examination further indicates that the position of the valley and peak in the Pt trace matches with the peak and valley peaks in the Pd trace, suggesting the formation of shells with alternating compositions of Pd and Pt. The XRD pattern further reveals that the triple-shelled nanocrystals are composed of Pd and Pt with a face-centered cubic structure (Figure S3, SI). Figure 3D shows a typical HRTEM image of an individual triple-shelled octahedron. The HRTEM image shows well-resolved, continuous fringes in the same orientation from the Pd core to the Pt and Pd shells, indicating that the multi-shelled nanocrystal is a single crystal due to an epitaxial relationship between Pd and Pt, as confirmed by the corresponding Fourier transform (FT) pattern (inset of Figure 3D). The lattice spacing between neighboring fringes in the Pd and Pt regions are 2.27 and 1.96 Å, respectively. These values are in good agreement with the distances between two adjacent {111} and {200} planes of face-centered cubic (*fcc*) Pd and Pt. We believe that the same crystal structure and negligible lattice mismatching between Pd and Pt (0.77%) are responsible for the formation of single-crystal Pd–Pt multishelled nanocrystals.

The size and shape of Pd–Pt multishelled nanocrystals could be readily controlled by varying the amounts of K_2PtCl_4 and/or Na_2PdCl_4. Figure S4 in SI shows TEM images of Pd@Pt core–shell nanocrystals obtained by adding different amounts of K_2PtCl_4 in the first step. It is clear that there was a morphological transition from cuboctahedrons to octahedrons, together with a size increase from 9 to 11 nm with increasing of the K_2PtCl_4 amount from 1.8 to 7.2 mg. We found that 14 mg of K_2PtCl_4 was the maximum amount for generating Pd@Pt core–shell nanocrystals in high purity and quality. Further increase of the K_2PtCl_4 amount (e.g., to 28 mg as shown in Figure S4D in SI) resulted in the formation of Pt nanocrystals (marked by arrows) due to homogeneous nucleation. In addition, we could control the size of Pd@Pt@Pd double-shelled nanocrystals in the second step by varying the amount of Na_2PdCl_4. As shown by the TEM images in Figure 4, the size of the Pd@Pt@Pd nanocrystals was increased from 14 to 18 nm when the amount of Na_2PdCl_4 was increased from 2.4 to 38.4 mg. It seems to be difficult to control the size of multishelled nanocrystals over a broad range by varying the amounts of salt precursors starting from the seeds with {111} facets on the surface. The strong binding effect of CA to the {111} facets of Pd and Pt was responsible for the size limitation of a nanocrystal enclosed by {111} facets.

In order to further clarify the heteroepitaxial growth between Pd and Pt, we also used Pt nanocubes as the seeds for the synthesis of Pt–Pd multishelled nanocrystals. Figure 5 shows TEM images of the products obtained in different stages. Figure 5A shows a TEM image of Pt nanocubes with an average size of 5 nm. After reacting for 9 h in a mixture containing the Pt nanocubes, Na_2PdCl_4, and CA, the nanocrystals became octahedrons with an average size of 20 nm (Figure 5B). The magnified TEM image (inset of Figure 5B) clearly shows that there was a single cubic Pt seed in the center of each core–shell octahedron. The Pt@Pd core–shell octahedron was formed via epitaxial growth of a Pd shell along ⟨100⟩ direction on the Pt cube in the presence of CA, which was similar to the result of a previous report.[12] In comparison with the epitaxial growth of Pd on {111} facets of Pd@Pt seeds (Figure 2C), the overgrowth of Pd on {100} facets of Pt seeds proceeded extensively, resulting in the enlarged size and morphological transition from cubes to

octahedrons due to the selective capping effect of CA for {111} facets. In the following step, Pt and Pd shells were formed through conformal overgrowth on the {111} facets of Pt@Pd octahedrons in the presence of CA, respectively, as shown in C and D of Figure 5. The magnified TEM images (insets of Figure 5, C and D) revealed that only a thin shell of Pt and Pd were heteroepitaxially generated due to the strong binding of CA to {111} facets. Taken together, Pt−Pd multishelled core−shell nanocrystals with an octahedral shape could also be synthesized from Pt seeds through layer-by-layer epitaxial overgrowth, with CA serving as both reducing and capping agents.

In summary, we have demonstrated epitaxial growth of multishelled nanocrystals with a octahedral or platelike shape by alternating the salt precursors added to a system containing Pd or Pt nanocrystals (the seed) and CA (as both reducing and capping agents). The slow reduction kinetics associated with CA played an important role in promoting layer-by-layer epitaxial growth for both Pt and Pd, and thus ensuring the formation of Pd−Pt multishelled nanocrystals. When the epitaxial growth was on {111} facets (e.g., for Pd octahedrons and plates), the shape of the seeds was essentially maintained, and the epitaxial shells were relatively thin. In contrast, extensive overgrowth was observed when nanocrystals (e.g., Pd cuboctahedrons and Pt cubes) with {100} facets exposed on the surface were employed as seeds, leading to the formation of thick shells, together with a transition in morphology. It is expected that these Pd−Pt multishelled nanocrystals, combining the properties from both Pd and Pt, may find uses in many applications such as catalysis (Figure S5, SI, formic acid oxidation with surface-dependent activity). We believe that the approach presented here can be extended to synthesize multishelled nanocrystals with other elemental compositions and distribution patterns for various applications.

■ ASSOCIATED CONTENT

Supporting Information. Experimental details, TEM images, XRD pattern, and CV curves of Pd−Pt multishelled nanocrystals. This material is available free of charge via the Internet at http://pubs.acs.org.

■ AUTHOR INFORMATION

Corresponding Author
xia@biomed.wustl.edu

■ ACKNOWLEDGMENT

This work was supported in part by a DOE subcontract from the University of Delaware (DE-FG02-03 ER15468), a research grant from the NSF (DMR-0804088), and startup funds from Washington University in St. Louis. As a visiting scholar from Zhejiang University, H.Z. was also partially supported by the "New Star Program" of Zhejiang University. J.W. and M.K. were supported by a grant from CNMT (2010K000336) under the 21st Frontier R&D Program of the MEST, Korea. Part of the research was performed at the Nano Research Facility, a member of the National Nanotechnology Infrastructure Network (NNIN), which is supported by the NSF (ECS-0335765).

■ REFERENCES

(1) Wang, L.; Clavero, C.; Huba, Z.; Carroll, K. J.; Carpenter, E. E.; Gu, D. F.; Lukaszew, R. A. *Nano Lett.* **2011**, *11*, 1237.
(2) Major, K.; De, C.; Obare, O. *Plasmonics* **2009**, *4*, 61.
(3) Lu, C.; Prasad, K.; Wu, H.; Ho, J.; Huang, M. *J. Am. Chem. Soc.* **2010**, *132*, 14546.
(4) Yamauchi, M.; Kobayashi, H.; Kitagawa, H. *ChemPhysChem* **2009**, *10*, 2566.
(5) Kobayashi, H.; Yamauchi, M.; Kitagawa, H.; Kubota, Y.; Kato, K.; Takata, M. *J. Am. Chem. Soc.* **2008**, *130*, 1818.
(6) Wang, F.; Sun, L.; Feng, W.; Chen, H.; Yeung, M.; Wang, J.; Yan, C. *Small* **2010**, *6*, 2566.
(7) Ferrer, D.; Torres-Castro, A.; Gao, X.; Sepulveda-Guzman, S.; Ortiz-Mendez, U.; Jose-Yacaman, M. *Nano Lett.* **2007**, *7*, 1701.
(8) Carbone, L.; Cozzoli, P. *Nano Today* **2010**, *5*, 449.
(9) Lim, B.; Kobayashi, H.; Yu, T.; Wang, J.; Kim, M.; Li, Z.; Rycenga, M.; Xia, Y. *J. Am. Chem. Soc.* **2010**, *132*, 2506.
(10) Wang, D.; Xin, H.; Yu, Y.; Wang, H.; Rus, E.; Muller, D.; Abruna, H. *J. Am. Chem. Soc.* **2010**, *132*, 17664.
(11) Zhang, J.; Tang, Y.; Weng, L.; Ouyang, M. *Nano Lett.* **2009**, *9*, 4061.
(12) Habas, S.; Lee, H.; Radmilovic, V.; Somorjai, G.; Yang, P. *Nat. Mater.* **2007**, *6*, 692.
(13) Lee, Y.; Kim, M.; Kim, Z.; Han, S. *J. Am. Chem. Soc.* **2009**, *131*, 17036.
(14) Xiang, Y.; Wu, X.; Liu, D.; Jiang, X.; Chu, W.; Li, Z.; Ma, Y.; Zhou, W.; Xie, S. *Nano Lett.* **2006**, *6*, 2290.
(15) Fan, F.; Liu, D.; Wu, Y.; Duan, S.; Xie, Z.; Jiang, Z.; Tian, Z. *J. Am. Chem. Soc.* **2008**, *130*, 6949.
(16) Lim, B.; Jiang, M.; Camargo, P.; Cho, E.; Tao, J.; Lu, X.; Zhu, Y.; Xia, Y. *Science* **2009**, *324*, 1302.
(17) Lim, B.; Wang, J.; Camargo, P.; Jiang, M.; Kim, M.; Xia, Y. *Nano Lett.* **2008**, *8*, 2535.
(18) Jiang, M.; Lim, B.; Tao, J.; Camargo, P.; Ma, C.; Zhu, Y.; Xia, Y. *Nanoscale* **2010**, *2*, 2406.
(19) Lim, B.; Jiang, M.; Tao, J.; Camargo, P.; Zhu, Y.; Xia, Y. *Adv. Funct. Mater.* **2009**, *19*, 189.
(20) Thomas, J.; Johnson, B.; Raja, R.; Sankar, G.; Midgley, P. *Acc. Chem. Res.* **2003**, *36*, 20.
(21) Tao, F.; Dag, S.; Wang, L.; Liu, Z.; Butcher, D.; Bluhm, H.; Salmeron, M.; Somorjai, G. *Science* **2010**, *327*, 850.
(22) Peng, Z.; Yang, H. *Nano Today* **2009**, *4*, 143.
(23) Zhang, H.; Jin, M.; Wang, J.; Li, W.; Camargo, P.; Kim, M.; Yang, D.; Xie, Z.; Xia, Y. *J. Am. Chem. Soc.* **2011**, *133*, 6078.
(24) Wang, Z. L. *J. Phys. Chem. B* **2000**, *104*, 1153.